STRUCTURAL ANALYSIS OF LAYERS OF PEROVSKITE SOLAR CELL BY USING SMARTLAB X-ray DIFFRACTOMETER

Hsan Htoo[1], Thiri Htet[2], Ye Chan[3]

Abstract

X-ray structure and crystallite size of fabricated layers of perovskite solar cell were investigated. The first layer, compact TiO_2 layer was deposited using a spray pyrolysis method. The structure TiO_2 is tetragonal and crystallite size of first TiO_2 layer is 43.20 nm. The second mesoporous TiO_2 was deposited by screen printing of TiO_2 slurry and the crystallite size is 53.10 nm. The third ZrO_2 space layer was printed on the top of the TiO_2 layer using ZrO_2 paste and the crystallite size is 33.26 nm. The structure of ZrO_2 is monoclinic. Then, a carbon counter electrode was coated on the top of the ZrO_2 layer by printing carbon slurry and the crystallite size is 27.00 nm. The $CH_3NH_3PbI_3$ perovskite layer was prepared by two-step solution method. The unit cell structure is tetragonal and the crystallite sizes lie between 22.30 nm to 27.40 nm. From XRD results, the lattice constants of $CH_3NH_3PbI_3$ are 8.86 Å and 12.66 Å. The bond distances among the atoms of perovskite layer are 2.66 Å at Pb1-I1, 3.15 Å at Pb1-I2 and 1.13 Å at C1-N1.

Keywords: perovskite, crystallite size, lattice parameter, bond distance

Introduction

In crystallography, crystal structure is a description of the ordered arrangement of atoms, ions or molecules in a crystalline material. Ordered structures occur from the intrinsic nature of the constituent particles to form symmetric patterns that repeat along the principal directions of three-dimensional space in matter. The smallest group of particles in the material that constitutes this repeating pattern is the unit cell of the structure. The unit cell completely reflects the symmetry and structure of the entire crystal, which is built up by repetitive translation of the unit cell along its principal axes. The translation vectors define the nodes of the Bravais lattice. The lengths of the principal axes, or edges, of the unit cell and the angles between them are the lattice constants, also called *lattice parameters* or *cell parameters*. The symmetry properties of the crystal are described by the concept of space groups. All possible symmetric arrangements of particles in three-dimensional space may be described by the 230 space groups. The crystal structure and symmetry play a critical role in determining many physical properties, such as cleavage, electronic band structure, and optical transparency.

Solar cells with a perovskite structure have high conversion efficiencies and stability as the organic solar cells. Since a photoconversion efficiency of 15% was achieved, higher efficiencies have been reported for various device structures and processes, and the photoconversion efficiency was increased up to 19.3%. The photovoltaic properties of solar cells are strongly dependent on the fabrication process, hole transport layers, electron transport layers, nanoporous layers, interfacial microstructures, and crystal structures of the perovskite compounds. Especially, the crystal structures of the perovskite-type compounds, strongly affect the electronic structures such as energy band gaps and carrier transport, and a detailed analysis of them is mandatory. The organic–inorganic hybrid perovskite materials such as $CH_3NH_3PbI_3$ can improve the solar conversion efficiency of DSCs (dye-sensitized solar cell). Several groups have

[1] Lecturer, Department of Physics (Attached URC), University of Yangon
[2] Department of Physics, Dagon University
[3] Universities' Research Centre, University of Yangon

shown that the perovskite morphologies such as the grain size and crystallinity highly affect the performance of solar cells [1]. Therefore, understanding the structures and crystallite size of these prototype light harvesters is important for the molecular design of organic–inorganic perovskite materials with defined properties. Each Pb^{2+} cation was coordinated to six I^- anions to form [PbI_6] octahedral. These [PbI_6] are corner connected to each other forming a three-dimensional Pb–I framework. Each $CH_3NH_3^+$ cation locates at the centre of four [PbI_6] octahedra. Thus, each cation interacts with twelve I^- anions. The symmetry and structure of $CH_3NH_3PbI_3$ crystals are highly dependent on the temperature. In this study, the crystallite size of layers of perovskite solar cell will be analysis at different temperatures.

Materials and Method

2.1 Materials

The materials fluorine-doped tin oxide (FTO) galss, titanium dioxide (TiO_2), zirconium oxide (ZrO_2), graphite, methyl ammonium iodide (MAI) (98% Sigma-Aldrich), lead II iodide (PbI_2), hydrochloric acid (HCL), ethanol, isopropanol, acetylacetone, acetic acid, acetonitrile, ethylene glycol and dimethyl formamide (DMF) were used in this research.

2.2 Experimental Procedure

2.2.1 Preparation of compact and mesoporous TiO_2 films (Electron Transporting Layer)

4g of TiO_2 powder, 40 ml of ethanol and 20 ml of distilled water were mixed in the beaker. Then it was continuously stirred by magnetic stirrer at 70°C for 2 h. Thereafter, TiO_2 solution was deposited onto the glass substrate by spray pyrolysis method for compact layer.

TiO_2 paste for mesoporous layer was prepared by addition of few 10-20 ml of ethanol to the TiO_2 powder and continuously stirred by a magnetic stirrer to until the desired paste is formed. Then TiO_2 mesoporous layer was printed on TiO_2 fine layer by using screen printing method.

2.2.2 Preparation of ZrO_2 film (Space layer)

2 g of ZrO_2 powder was mixed with 20 ml of ethanol and 2 ml of isopropanol in the beaker. Then the solution was stirred by magnetic stirrer at 70°C to make a viscous paste for screen printing on the mesoporous TiO_2 layer.

2.2.3 Preparation of graphite layer (Counter Electrode –CE)

2g of graphite powder, acetylacetone, acetic acid, acetonitrile, ethylene glycol 1.5 ml each were ground by using motor and pestle for 3h to form a paste for blade coating (doctor blading) method.

2.2.4 Making the perovskite precursor solution

In the case of the inter-diffusion reaction (sequential deposition) of the inorganic and organic precusors, the PbI_2 precursor is dissolved in dimethylformamide (DMF) (400 mg/ ml) and stirred at 70° C for 30 minutes. CH_3NH_3I precursor is dissolved in isopropanol (IPA) at a concentration of 10 mg/ ml.

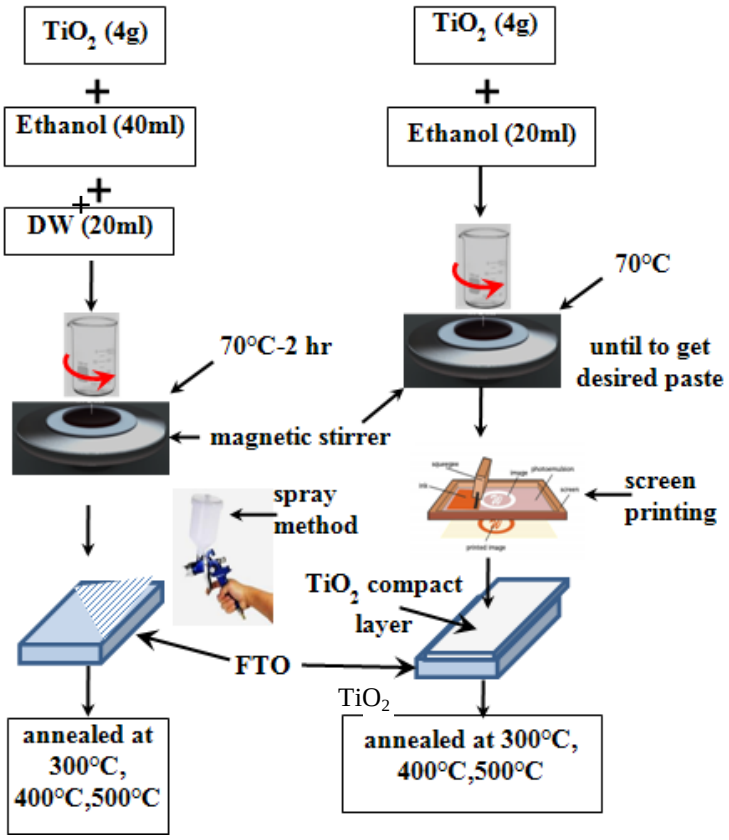

Figure 1 Preparation of compact TiO_2 & mesoporous TiO_2 films

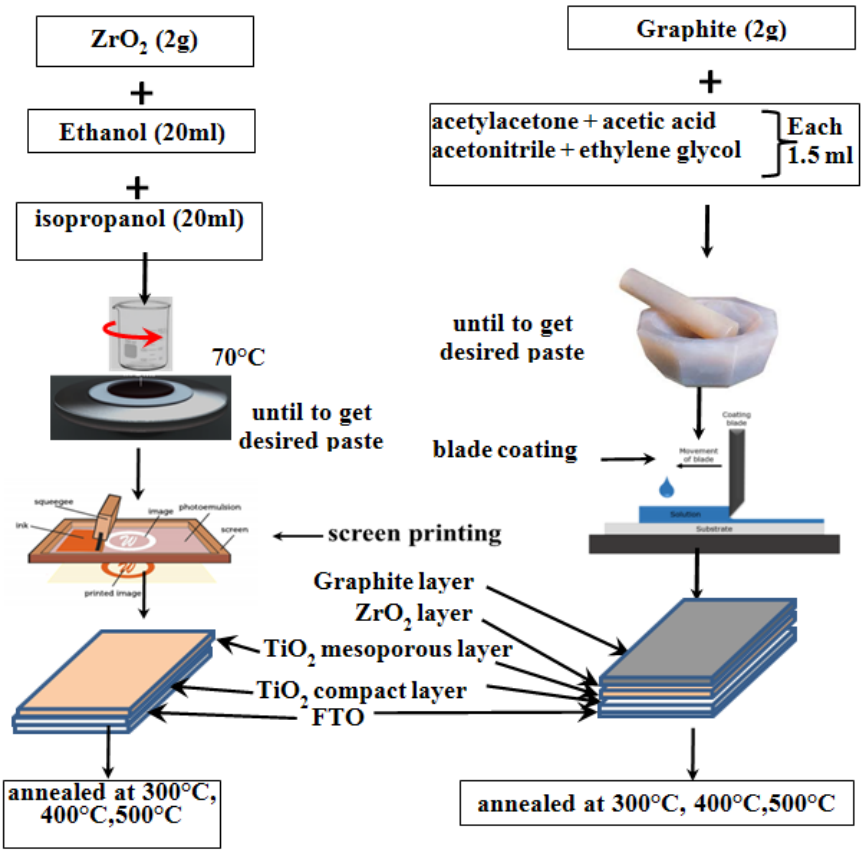

Figure 2 Preparation of ZrO_2 & Graphite films

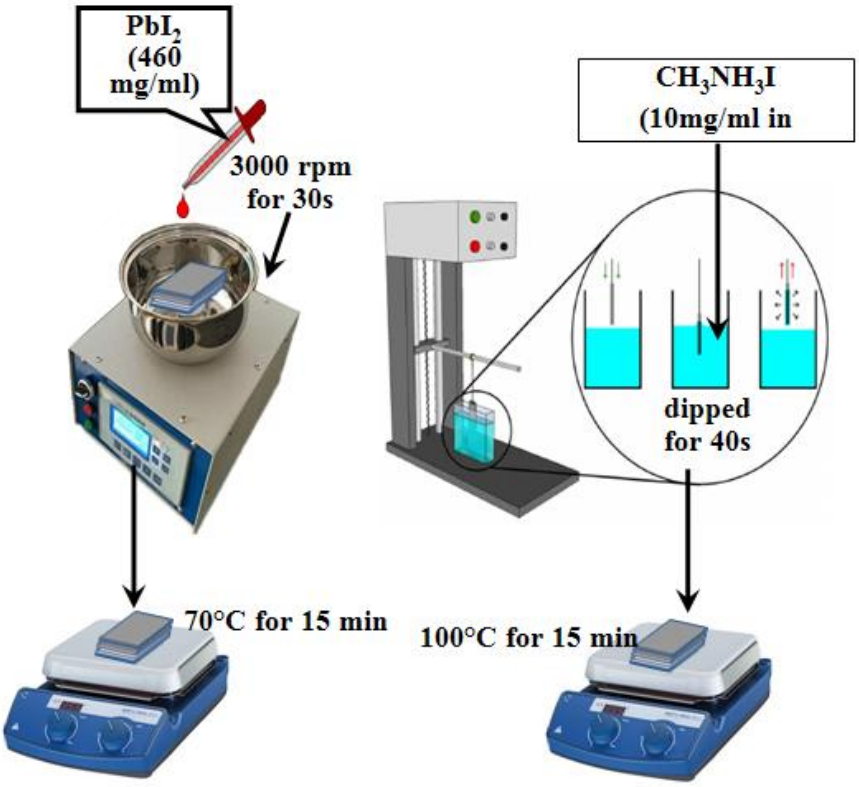

Figure 3 Preparation of perovskite films

2.3 Fabrication of Photovoltaic Devices

The (FTO) coated glass substrates were cleaned by soaking in the mix solution of HCl and distilled water (1:10 ratio) for 30 minutes. And then it was rinsed in DI water and dried in room temperature. After that, the substrates were coated with compact TiO_2 layer by aerosol spray pyrolysis and annealed at 300 °C, 400°C and 500°C for 30 minutes respectively. After that the mesoporous TiO_2 layer was deposited on top of the compact layer by screen printing and sintered at 300°C, 400°C and 500°C for 30 minutes respectively. Followed, ZrO_2 space layer was printed by screen printing and the films were sintered at 300°C, 400°C and 500°C for 30 minutes respectively. After cooling down, graphite CE was prepared by doctor-blade coating on the ZrO_2 space layer and followed by heating at 300°C, 400°C and 500°C for 30 minutes respectively. To prepare $CH_3NH_3PbI_3$ perovskite films, the PbI_2 solution (460 mg/ml in DMF) was spin coated on the mesoporous graphite layer at 3000 rpm for 30 s and dried at 70°C for 15 minutes. Then the substrates were dipped into CH_3NH_3I solution (10 mg/ml in isopropanol) for 40s. After that, it was heated for 15 minutes at 100º C on a hot plate. During the procedure, the coated electrode changed color from light yellow to dark brown, indicating the formation of the perovskite film.

X-ray Data Collection and Characterization

XRD data collection was carried out using SmartLab X-ray diffractometer. As an X-ray source, Cu-Kα radiations were used with the X-ray power of 50kV × 40 mA. The detector was semiconductor detector. All measurements were performed by a 2θ scan method. The range of 2θ in which intensity data were collected was between 10˚ to 70˚.

The structures of crystals and molecules are often being identified using x-ray diffraction studies, which are explained by Bragg's Law. The law explains the relationship between an x-ray light shooting into and its reflection off from crystal surface. The Bragg's law states that when the x-ray is incident onto a crystal surface, its angle of incidence, θ, will reflect back with a same angle of scattering, θ. And, when the path difference, d is equal to a whole number, n, of wavelength, a constructive interference will occur. Knowing the wavelength and the diffraction angle of a reflection, its resolution *d* can be easily calculated:

$$d= 1/2(n\lambda/ \sin\theta)$$

This is just a reformulation of the famous Bragg equation $n\lambda= 2d \sin\theta$.

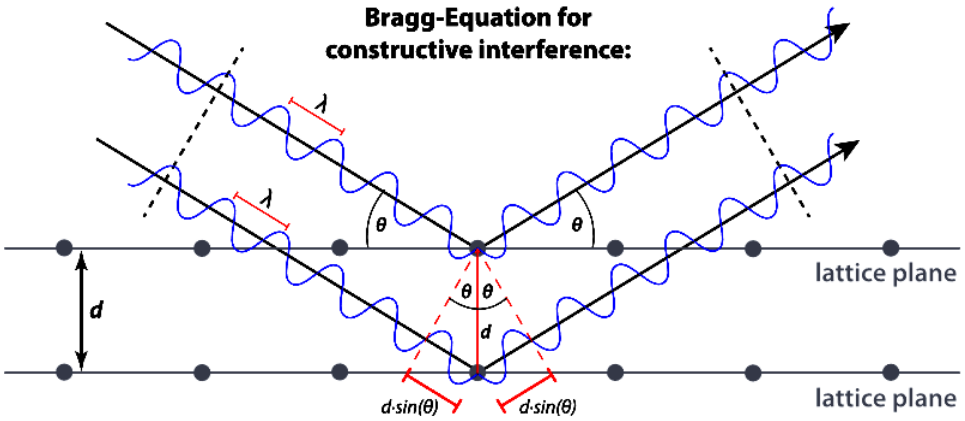

Figure 4 Bragg-Equation for Constructive Interference

The structural analysis of perovskite layer was performed using Smart Lab Studio II software. The crystallite size of solar cell layers were carried out by using the Debye-Scherrer formula.

$$D = \frac{0.9\ \lambda}{B \cos\theta}$$

Where, D = Crystallite size (nm)

λ = the wavelength of X-ray used (1.54056 Å)

B = Full Width Half Maximum of dominant peak (radian)

θ = Angle of diffraction (radian)

The interplanar spacing d between (h k l) lattice planes for seven crystal system are can be calculated by using following formulae.

Cubic:

$$\frac{1}{d^2}=\frac{h^2+k^2+l^2}{a^2}$$

Tetragonal:

$$\frac{1}{d^2}=\frac{h^2+k^2}{a^2}+\frac{l^2}{c^2}$$

Hexagonal:

$$\frac{1}{d^2}=\frac{4}{3}\left(\frac{h^2+hk+k^2}{a^2}\right)+\frac{l^2}{c^2}$$

Rhombohedral:

$$\frac{1}{d^2}=\frac{(h^2+k^2+l^2)\sin^2\alpha+2(hk+kl+hl)(\cos^2\alpha-\cos\alpha)}{\alpha^2(1-3\cos^2\alpha+2\cos^3\alpha)}$$

Orthorhombic:

$$\frac{1}{d^2}=\frac{h^2}{a^2}+\frac{k^2}{b^2}+\frac{l^2}{c^2}$$

Monoclinic:

$$\frac{1}{d^2}=\left(\frac{h^2}{a^2}+\frac{k^2\sin^2\beta}{b^2}+\frac{l^2}{c^2}-\frac{2hl\cos\beta}{ac}\right)\frac{1}{\sin^2\beta}$$

Triclinic:

$$\frac{1}{d^2}=\frac{\frac{h^2}{a^2}\sin^2\alpha+\frac{k^2}{b^2}\sin^2\beta+\frac{l^2}{c^2}\sin^2\gamma+\frac{2kl}{bc}(\cos\beta\cos\gamma-\cos\alpha)+\frac{2hl}{ac}(\cos\gamma\cos\alpha-\cos\beta)+\frac{2hk}{ab}(\cos\alpha\cos\beta-\cos\gamma)}{1-\cos^2\alpha-\cos^2\beta-\cos^2\gamma+2\cos\alpha\cos\beta\cos\gamma}$$

Results and Discussion

4.1 TiO_2 compact layers

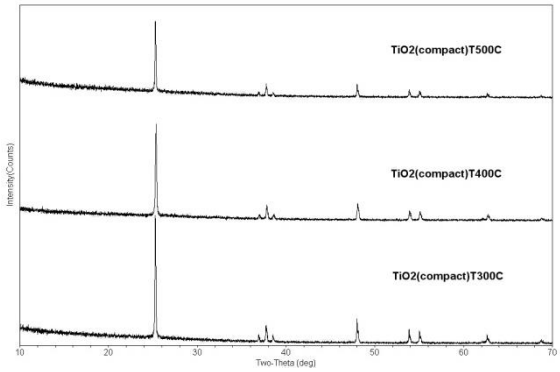

(a)

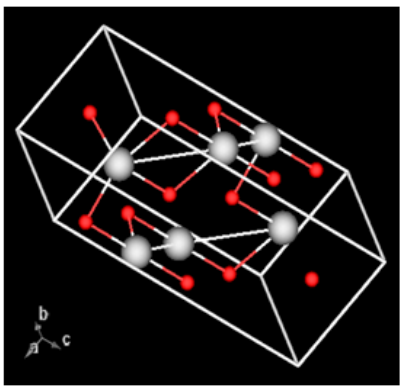

(b)

Figure 5 (a) XRD patterns of TiO_2 (compact) films at different temperatures (b) Unit cell structure of TiO_2

Table 1 The average crystallize size and lattice parameter of compact TiO_2 at 300˚C, 400˚C, 500˚C

No.	Temperature (˚C)	Lattice constant (Å)		Crystallize size (nm)	
		a	c	XRD	Calculation
1.	300	3.79	9.51	78.10	57.40
2.	400	3.77	9.55	50.40	43.20
3.	500	3.79	9.52	65.00	50.40

The XRD spectrum of compact TiO_2 layer at temperature 300°C, 400°C and 500°C were indicated in Fig.5.(a). The diffracted peaks are (101), (103), (004), (112), (200), (105), (211), (213), (204) and (116). All peaks were well matched with those of the standard JCPDS library file of anatase TiO_2. XRD patterns indicate that the crystal structures of TiO_2 were tetragonal structure. The crystallize size and lattice constant of compact TiO_2 at 300°C, 400°C and 500°C were tabulated in Table 1.

4.2 Mesoporous TiO_2 Layer

The crystallize size and lattice constant of mesoporous TiO_2 at 300°C, 400°C and 500°C were tabulated in Table 2.

Table 2 The average crystallize size and lattice parameter of mesoporous TiO_2 at 300˚C, 400˚C, 500˚C

No.	Temperature (˚C)	Lattice constant (Å)		Crystallize size (nm)	
		a	c	XRD	Calculation
1.	300	3.79	9.51	68.60	53.10
2.	400	3.78	9.52	71.40	53.90
3.	500	3.80	9.51	70.90	54.30

4.3 ZrO_2 space layers

XRD pattern of ZrO_2 layers for temperature of 300°C, 400°C and 500°C were shown in Fig.6. (a). From the XRD results, the crystal structures of ZrO_2 layers were monoclinic. The crystallize sizes and lattice constant were tabulated in Table 3.

Table 3 The average crystallize size and lattice parameter of ZrO_2 at 300˚C, 400˚C, 500˚C

No.	Temperature (˚C)	Lattice constant (Å)			Crystallize size (nm)	
		a	b	c	XRD	Calculation
1.	300	5.19	5.21	5.36	41.82	35.46
2.	400	5.16	5.21	5.35	36.58	33.26
3.	500	5.17	5.21	5.33	44.32	38.78

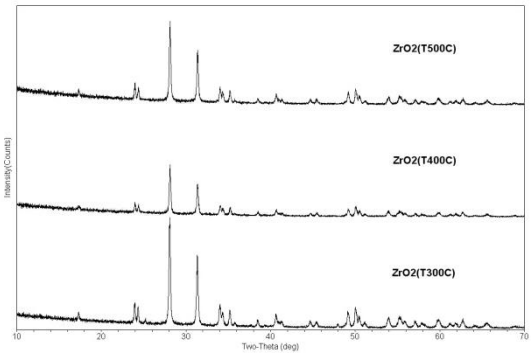

(a)

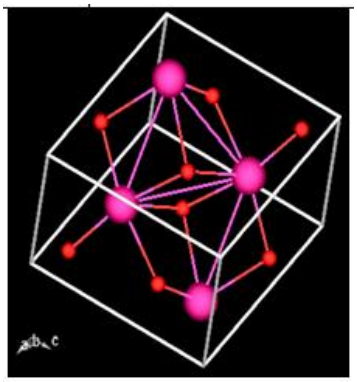

(b)

Figure 6 (a) XRD patterns of ZrO_2 (space layers) at different temperatures
(b) Unit cell structure of ZrO_2

4.4 Graphite layer (CE)

Fig.7. (a) showed the XRD profile of graphite layer at 300°C, 400°C and 500°C and unit cell structure. XRD patterns indicate that the crystal structures of graphite layers were hexagonal. The crystallize size and lattice constant of graphite at 300°C, 400°C and 500°C were tabulated in Table 4.

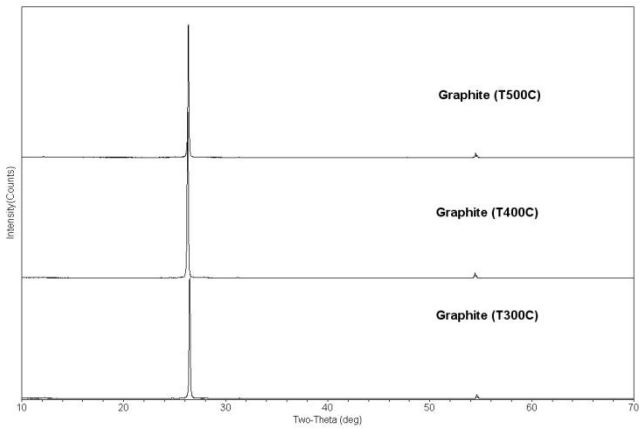

(a)

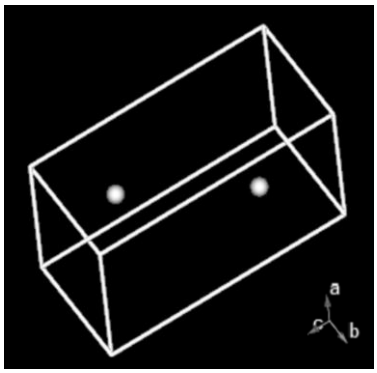

(b)

Figure 7(a)XRD patterns of graphite layer at different temperatures
(b) Unit cell structure of graphite

Table 4 The average crystallize size and lattice parameter of carbon layers at 300˚C, 400˚C, 500˚C

No.	Temperature (˚C)	Lattice constant (Å)		Crystallize size (nm)	
		a	c	XRD	Calculation
1.	300	2.46	6.73	41.40	33.60
2.	400	2.46	6.77	51.64	39.72
3.	500	2.46	6.75	28.80	27.00

4.5 Perovskite layer

In this work, a two-step spin coating method was used for the preparation of the $CH_3NH_3PbI_3$ perovskite layers. The XRD patterns of perovskite layers are as follow.

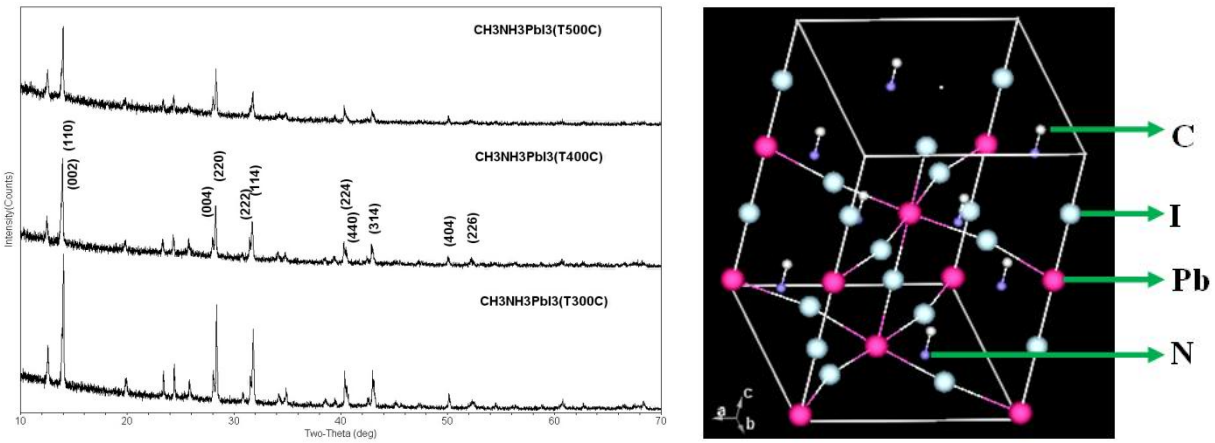

(a) (b)

Figure 8 (a) XRD patterns of perovskite layer at different temperatures (b) Unit cell structure of perovskite

Table 5 The average crystallize size and lattice parameter of perovskite layers at 300˚C, 400˚C, 500˚C

No.	Temperature (˚C)	Lattice constant (Å)		Crystallize size (nm)	
		a	c	XRD	Calculation
1.	300	8.89	12.66	26.8	24.9
2.	400	8.89	12.66	30.0	27.4
3.	500	8.86	12.66	23.4	22.3

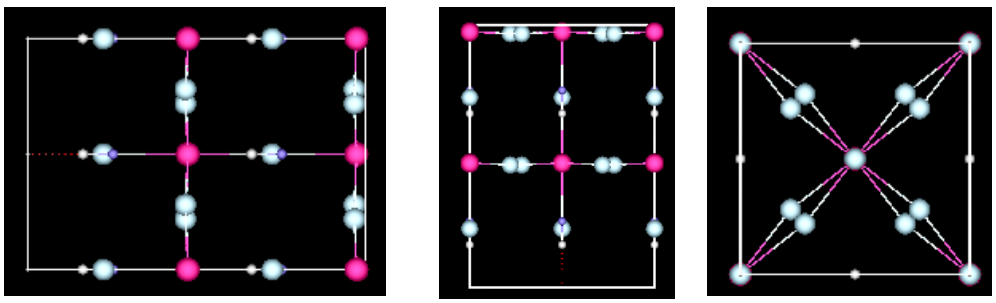

(a) (b) (c)

Figure 9 Unit cell structure of $CH_3NH_3PbI_3$ with view direction at (a) "**a**",(b) "**b**" (c) "**c**"

XRD pattern of $CH_3NH_3PbI_3$ layers for temperature of 300°C, 400°C and 500°C was shown in Fig.8. (a) Dominant peaks of (110), (004), (220), (114), (224), (400), (404) occur at diffraction angles of 13.957˚, 19.96˚, 23.339˚, 31.711˚, 40.298˚, 40.744˚, 50.045˚. The other peaks were PbI_2. The crystallize size and lattice constant were tabulated in Table 4. From the XRD results, the crystal structure of $CH_3NH_3PbI_3$ layer was tetragonal.

Structural Analysis for $CH_3NH_3PbI_3$ Perovskite Layer

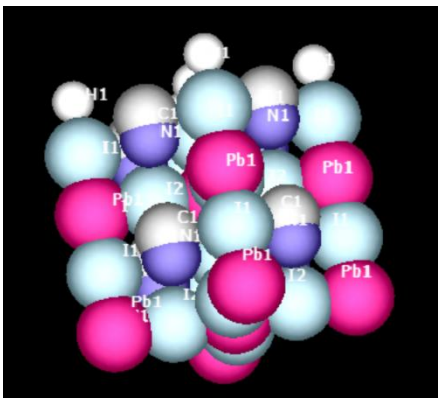

Figure 10 Space Filling Structure

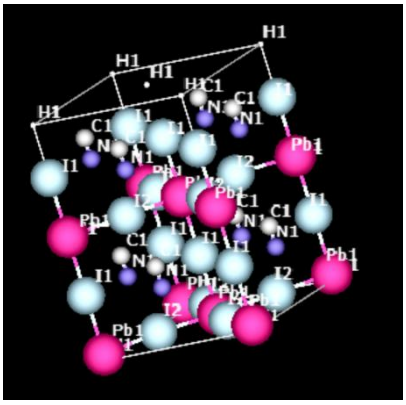

Figure 11 Ball & Stick Style

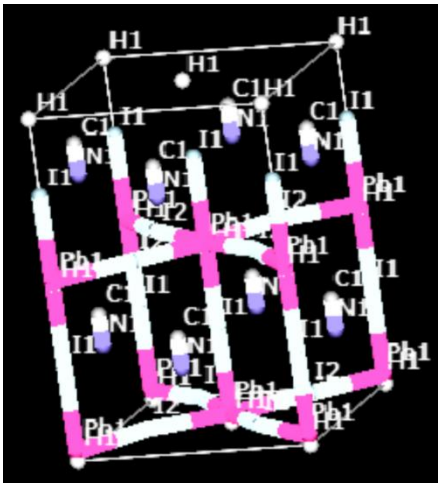

Figure 12 Cylinder Style

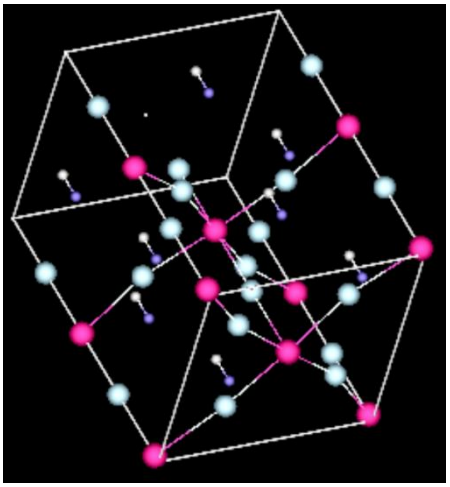

Figure 13 Line Style

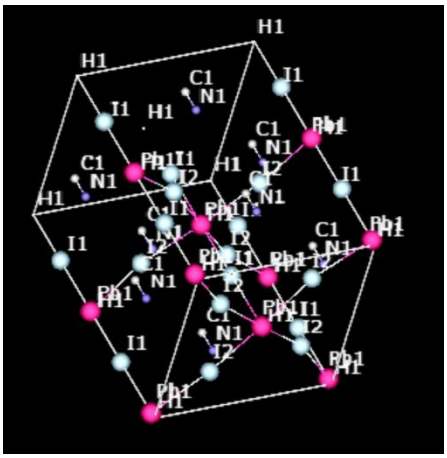

Figure 14 Marker Style

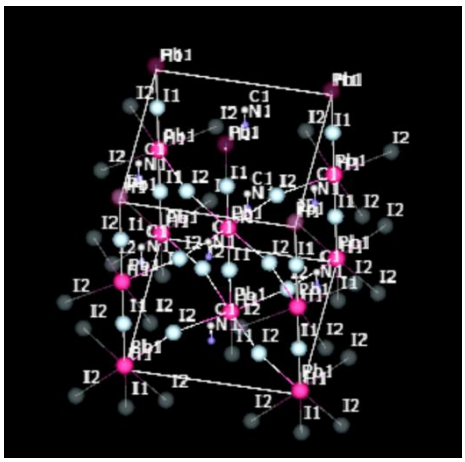

Figure 15 Expanding Style

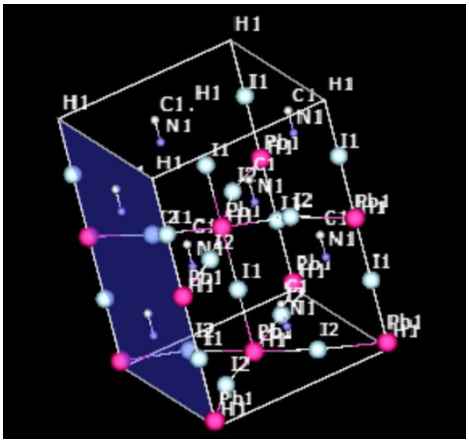

Figure 16 (100) plane

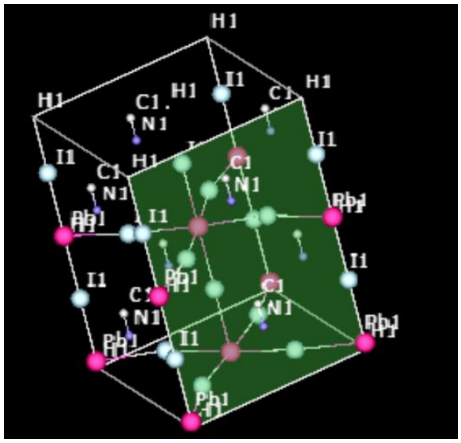

Figure 17 (010) plane

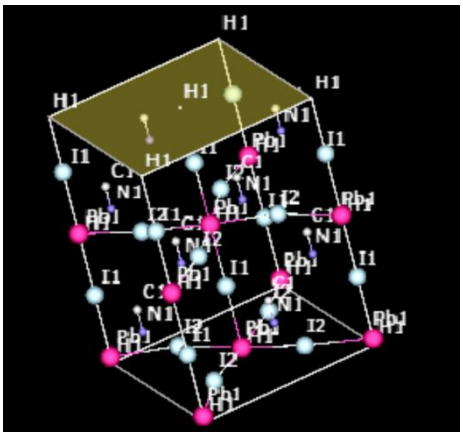

Figure 18 (001) plane

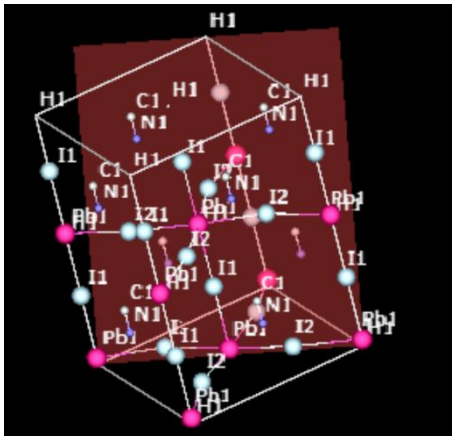

Figure 19 (111) plane

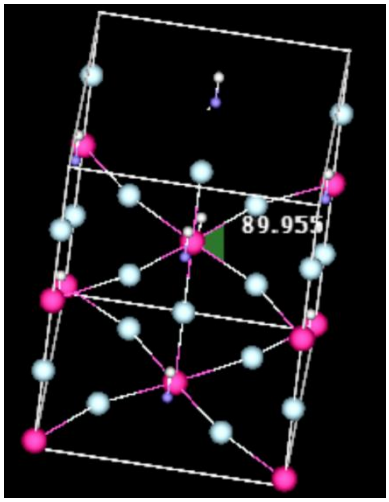

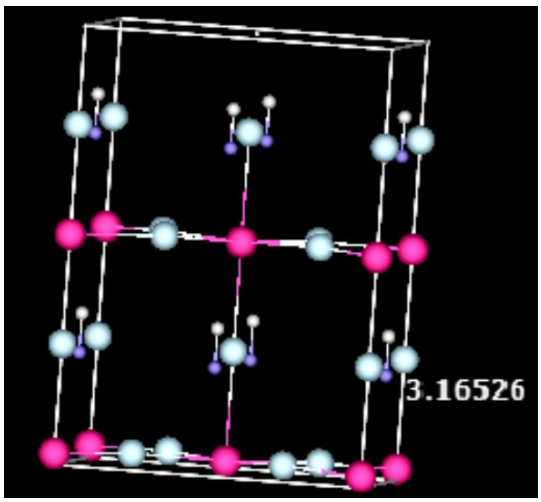

Figure 20 Determination of bond distance between atoms and angle between bond lengths

In this research, hole transporting layer free perovskite solar cell with graphite counter electrode was successfully fabricated by infiltrating of $CH_3NH_3PbI_3$ which consists of four layers including compact TiO_2, mesoporous TiO_2, ZrO_2 and graphite layers. The perovskite layer was deposited by two-step deposition technique. The energy band gap of the methyl ammonium lead iodide perovskite layers are 1.5 eV, 1.48 eV, 1.42 eV at different temperatures 500˚C, 300˚C and 400˚C with crystallize sizes of 23.41 nm, 26.75 nm and 30 nm. It was found that the highest

energy band gap value can get at 500 ˚C and smallest crystallize size was 23.41 nm. From XRD results, the lattice constants of $CH_3NH_3PbI_3$ are 8.86 Å and 12.66 Å. The bond distances among the atoms of perovskite layer are 2.66 Å at Pb1-I1, 3.15 Å at Pb1-I2 and 1.13 Å at C1-N1.

Acknowledgements

I would like to thanks Professor Dr Ye Chan, Professor and Head, Universities' Research Centre, University of Yangon, for his kind permission to carry out this work.

References

K. P. Ong, T. W. Goh, Q. Xu and A. Huan, J. Phys. Chem. A, (2015)

R. K. Singh, R. Kumar, N. Jain, J. Singh and S. K. Mishra, AIP Conference Proceedings, (2018)

W. Geng,C. Tong, J. Liu, W. Zhu, W. Lau, and L. Liu, Sci Rep. (2016) 6

T. Baikie, Y. Fang, J. M. Kadro, M. Schreyer, F. Wei, S. G. Mhaisalkar, Grätzel, M. & Whitec, T. J. (2013). Journal of Materials Chemistry A, Vol. 1, pp. 5628–5641

F. Hao, C. C. Stoumpos, D. H. Cao, R. P. H. Chang, and M. G. Kanatzidis (2014), Vol. 8, pp. 489-494.

Y. Kawamura, H. Mashiyama, and K. Hasebe, (2002). Journal of the Physical Society of Japan, Vol. 71, pp.1694–1697.

H. Mashiyama, Y. Kurihara, and T. Azetsu, (1998), Journal of the Korean Physical Society, Vol. 32, pp. S156–S158

https://en.wikipedia.org/wiki/crystal_structure